DOI: 10.1021/ma9023747

Macromolecules
ARTICLE

# Poly(thiophene) Nanoparticles Prepared by $Fe^{3+}$-Catalyzed Oxidative Polymerization: A Size-Dependent Effect on Photoluminescence Property

**Sun Jong Lee,[†] Jung Min Lee,[‡] Hak-Ze Cho,[†] Won Gun Koh,[†] In Woo Cheong,*[,§] and Jung Hyun Kim*[,†]**

[†]*Department of Chemical and Biomolecular Engineering, Yonsei University, 134 Shinchon-Dong, Seodaemoon-Gu, Seoul 120-749, Republic of Korea,* [‡]*Department of Chemical Engineering, Stanford University, Stanford, California 94305, and* [§]*Department of Applied Chemistry, Kyungpook National University, 1370 Sankyuk-dong, Buk-gu, Daegu 702-701, Republic of Korea*

*Received October 26, 2009; Revised Manuscript Received January 18, 2010*

ABSTRACT: Poly(thiophene) (PTh) nanoparticles with various sizes were directly prepared by $Fe^{3+}$-catalyzed oxidative polymerization of thiophene with varying hydrogen peroxide ($H_2O_2$) concentrations. In the polymerization, the $FeCl_3/H_2O_2$ (catalyst/oxidant) combination system was used as an initiator couple. Under the optimized reaction condition, percentage monomer conversions were >90%. With increasing $H_2O_2$ molar concentration from 2.35 to 5.88 M, the average sizes of the PTh nanoparticles decreased from 51 to 12 nm, and their photoemission wavelengths shifted from red to blue color at the maximum excitation wavelength ($\lambda^{UV}_{max}$ = 400 nm). However, the molecular weights of all PTh nanoparticles were ~3500 g/mol. As a result, we could tune the emitting colors that resulted from variations of the effective conjugation chain length by manipulating the size of PTh nanoparticles.

## Introduction

Polythiophene (PTh) and its derivatives are a class of conjugated polymers. Their optical and electrical properties in the bulk solid state have been studied extensively because of their high potential for the applications of electronic and optoelectronic devices, such as field-effect transistors,[1,2] light-emitting diodes,[3,4] and solar cells.[5,6] It is well known that their spectroscopic properties are closely related to coil-like, planar, and distorted conformations of the polymer chain.[7−9] In the coil-like conformation, twisted adjacent thiophene rings make the conjugation length short and its distribution broad, resulting in blue-shifted and structureless absorption and fluorescence spectra as compared with the planar conformation, where the thiophene rings are coplanar and the rotating motion is highly limited, that is, making the conjugation length longer and its distribution narrow. For example, Masuhara et. al demonstrated that a difference in polymer conformations and their spatial arrangements evolved into a difference in the nanometer-scaled surface morphology of poly(3-[2-(*N*-dodecylcarbamoyloxy)ethyl]-thiophene-2,5-diyl) (P3DDUT) films.[10−12]

In our previous studies, we proposed a synthetic mechanism for the formation of PTh nanoparticles prepared by $Fe^{3+}$-catalyzed oxidative polymerization in aqueous medium. This method includes a $FeCl_3/H_2O_2$ (catalyst/oxidant) combination system, which can make roughly 30 nm PTh nanoparticles with only a trace of $FeCl_3$.[13] Herein, we report a simple procedure for preparing PTh nanoparticles with controllable particle sizes. The presence of sodium dodecyl sulfate (SDS) in the reaction medium allows the size of PTh nanoparticles to be controlled by varying the concentration of $H_2O_2$. The higher the concentration of $H_2O_2$, the smaller the resulting polymer particles. We investigated particle size dependence on absorption and fluorescence spectra and considered these novel phenomena to arise from a difference in polymer conformations and spatial arrangements. Moreover, we found that the PTh nanoparticles showed a nanometer surface protrusion accompanying the blue shift in the fluorescence spectrum upon near-field excitation.

The particles are insoluble in both water and organic solvents and do not form colloidal dispersions. This is an advantage over colloidal PTh particles for certain applications.[14−16] Because of their insolubility, they can be easily and quickly separated from the reaction medium and washed using either filtration or centrifugation. Our procedure is also easy to wash and control particle size. Moreover, it is much cheaper than template-fabrication methods, where the cost of the template may limit the commercial availability.

## Experimental Section

**Materials.** Thiophene monomer (Acros Organics) was refrigerated at −5 °C until use. SDS (Samchun Pure Chemical) was purchased and used as received without further purification. Anhydrous ferric chloride ($FeCl_3$, Kanto Chemical) and hydrogen peroxide ($H_2O_2$, 50%, DC Chemical) were used as catalysts and oxidants, respectively. They were dried at 20 °C in the vacuum oven before use. They were all analytical grade and used without further purification. Pure water (>18.2 M·cm, Millipore) was used throughout the experiments.

**Preparation of Polythiophene Nanoparticles.** $Fe^{3+}$-catalyzed oxidative polymerization of thiophene was carried out in a 250 mL double-jacketed glass reactor, equipped with a mechanical stirrer, a thermometer, a reflux condenser, a temperature controller, an initiator funnel, and a nitrogen inlet. The basic recipe used for the polymerization was given in the Supporting Information (Table S1). The reactor was charged with the desired amount of 16.0 g thiophene monomer, 8.00 g SDS, 32.0−80.0 g $H_2O_2$, and 200 g pure water. Then, we added 0.032 g of the $FeCl_3$ aq solution to the reactor by using the initiator

*Corresponding authors. (J.H.K.) Tel: +82-2-2123-7633. Fax: +82-2-312-0305. E-mail: jayhkim@yonsei.ac.kr. (I.W.C.) Tel: +82-53-950-7590. Fax: +82-53-950-6594. E-mail: inwoo@knu.ac.kr.

 Published on Web 02/09/2010 © 2010 American Chemical Society

**Scheme 1. Schematic Illustration of the Mechanism for the Aromatic Nitration of Polythiophene**

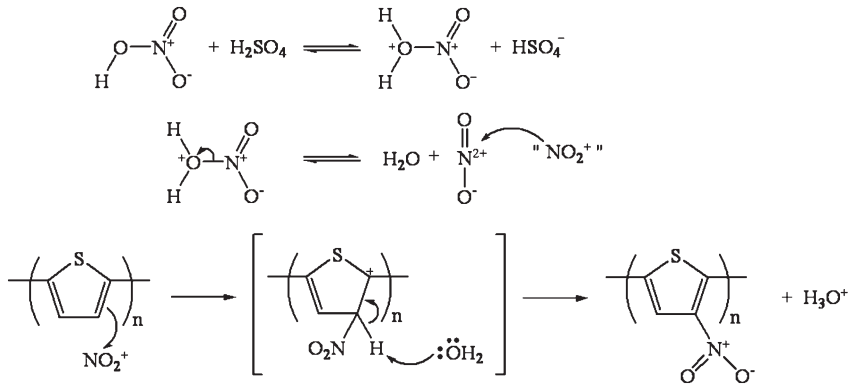

funnel. Highly pure nitrogen gas was purged for 30 min to remove dissolved oxygen in the reaction mixture. We initiated the polymerization by dropping the initiator solution, which had been deoxygenated with the nitrogen gas. Reaction temperature was adjusted to 50 ± 1 °C in a thermostat water bath. The stirring rate was kept at 300 rpm.

**Nitration of Polythiophene Nanoparticles.** Nitration of the pristine PTh nanoparticles was carried out to measure the molecular weight because of the poor solubility of the pristine PTh (unsubstituted) nanoparticles in organic solvents.[17] First, the sample of PTh nanoparticles was taken from the polymerization mixture at regular intervals. Then, an excess amount of the mixed acid (95% $H_2SO_4$/61% $HNO_3$/$H_2O$ 1.00:0.17:0.13 v/v) was added to the PTh nanoparticles, and the mixture was stirred for 4 h at 40 °C. After cooling to room temperature, the mixture was poured in cold water. The nitrated PTh was collected by filtration, washed with water, and then dried under vacuum.[18] A schematic illustration of the mechanism for the aromatic nitration of PTh was shown in Scheme 1.

## Characterization

**Surface Tension Measurements.** The surface tension measurement (Surface Tension 21 model, Fisher Scientific Instruments) was performed on the du Noüy ring method to determine the critical micelle concentration (CMC) of SDS in the $H_2O_2$-rich polymerization medium (0.0−20 wt % based on water) at 25 ± 1 °C.

**Solid Content and Particle Size of the Polythiophene Nanoparticles.** The solid content of the final latex, as determined by a gravimetrical analysis method, was 9.23 wt %. The average particle size ($D_n$: number-average) was obtained by using a transmission electron microscope (TEM; JEM-2000EXII, JEOL, Japan) and field emission scanning electron microscope (FE-SEM; JSM-600F, JEOL) equipped with image analysis software by over 500 particles with a low magnitude image. All samples were measured after cleaning by dialysis.

**Molecular Weight and Molecular Weight Distribution of the Nitrated Polythiophene.** The average molecular weights and molecular weight distribution of the nitrated PTh were measured by using a gel permeation chromatography (GPC, Waters Co.) equipped with a series of Waters columns (HR4, HR3, HR2, HR1), HPLC pump, RI detector, and data module at 40 °C. Molecular weights were determined from the refractive index data, which were analyzed with Waters Breeze System. Polystyrene standards and universal calibration were adapted to reduce the measuring error. Eluent was tetrahydrofuran (THF) with a flow rate of 1.0 mL/min.

**Chemical Structure Analysis of Polythiophene Nanoparticles.** The chemical structure of the PTh nanoparticles was observed with Fourier transform infrared spectroscopy (FT-IR; TENSOR27, Bruker Optik GmbH, Germany) in a range of 400−4000 $cm^{-1}$ at room temperature. For investigation of the aromatic nitration of the PTh nanoparticles, all samples were exposed to nitric ($HNO_3$) and sulfonic ($H_2SO_4$) acid for 4 h. Afterward, the samples were dried and analyzed by the use of FT-IR.

**Degree of Nitration of Polythiophene Nanoparticles.** The degree of nitration of the PTh nanoparticles was measured by elemental analysis.[18] The degree of nitration was calculated from the nitrogen/carbon (N/C) molar ratio obtained in elemental analysis. Elemental analysis was carried out with a LECO CHNS-932 analyzer and a Yanaco YS-10 SX-Elements microanalyzer. Inductively coupled plasma emission spectrometry (ICP-AES) of Ni, Mg, and Li was carried out using a Shimadzu ICPS-8100 apparatus.

**Photoluminescence Properties of the Polythiophene Nanoparticles.** The UV−visible absorption spectra were obtained in a UV−vis spectrophotometer (UV-1601PC, Shimadzu). Photoluminescence spectra were recorded with a spectrofluorophotometer (RF-5301PC, Shimadzu). The excitation was incident at an angle of 0° onto the front face of the sample, and the emission was recorded in reflection at an angle of 90° with respect to the surface normal.

## Results and Discussion

In this work, the particle formation of PTh takes place in the SDS micelles.[13] The size or number of PTh nanoparticles would be varied with the number of micelles, which can be controlled by the $H_2O_2$ concentration. To analyze the CMC of SDS in $H_2O_2$ rich aq solution, the surface tension measurement was carried out with varying the $H_2O_2$ concentration from 0.00 to 7.06 M (Figure S2 of the Supporting Information).

Figure 1 shows the CMC values of SDS in $H_2O_2$ aq solution as a function of $H_2O_2$ concentration. The CMC values can be assumed to be in the range of 0.00−7.06 M $H_2O_2$ solutions at 25 °C. This CMC value (1.07 mM) found for SDS in 5.88 M $H_2O_2$ solution or more is smaller than the value (8.32 mM) in pure water (at 25 °C) taken as a reference.[19,20] From these results, it was concluded that $H_2O_2$ would induce and promote to make micelle formations of SDS in aqueous medium. Consequently, at a high concentration of $H_2O_2$ solution, a number of the micelles exist in the aqueous phase, and those grow to be nanoreactor domain.

Figure 2 shows the time−conversion curves for the $Fe^{3+}$-catalyzed oxidative polymerization of thiophene in $H_2O_2$ aq solution as a function of $H_2O_2$ concentration. The final percent conversions of thiophene monomer are >90% in all cases. The reaction rates rapidly increased in the beginning of the polymerization; however, the rates decreased with the lapse of time and were significantly affected by the concentration of $H_2O_2$. These

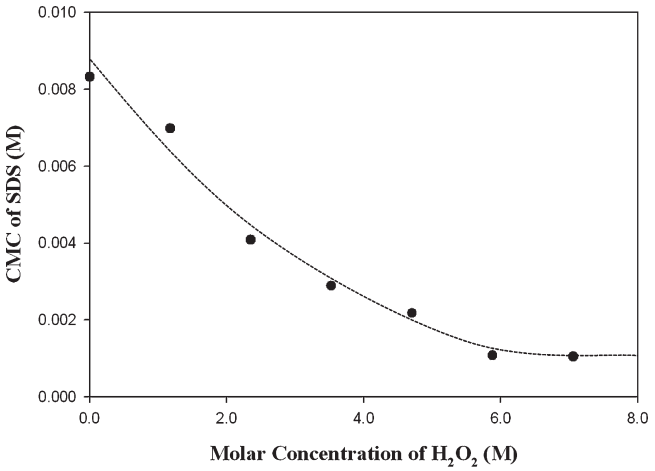


**Figure 1.** CMC values of SDS in $H_2O_2$ aq solution as a function of $H_2O_2$ concentration.

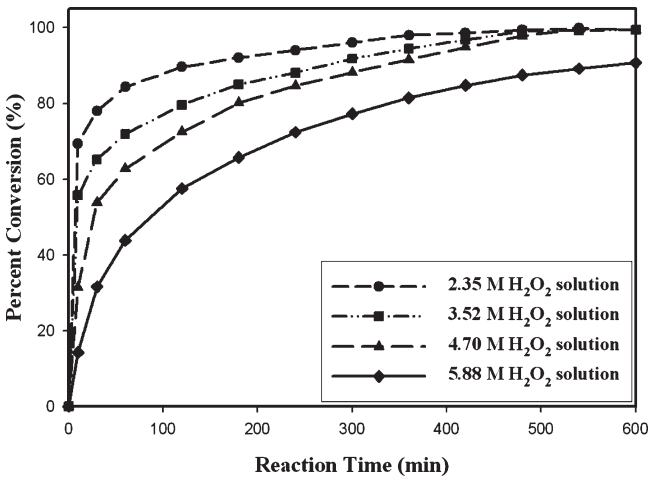


**Figure 2.** Time−conversion curves for PTh nanoparticles prepared by $Fe^{3+}$-catalyzed oxidative polymerization in $H_2O_2$ aq solutions: 2.35 M $H_2O_2$ solution (●), 3.52 M $H_2O_2$ solution (■), 4.70 M $H_2O_2$ solution (▲), and 5.88 M $H_2O_2$ solution (♦).

phenomena can be explained by the number of $Fe^{3+}$ ions. At the high concentration of $H_2O_2$ solution, SDS can make more micelles because of the lower CMC, which leads to the larger interfacial area of the micelles. At this moment, $Fe^{3+}$ ions exist on the periphery of the monomer-swollen micelle surface because of the electrostatic attraction between sulfate ($OSO_3^-$) groups and $Fe^{3+}$ ions, and the polymerization is driven by the reaction between the $Fe^{3+}$ ions and thiophene monomer.[13] However, the number of $Fe^{3+}$ ions per a micelle would be very small because the limited (0.197 mmol) amount of $Fe^{3+}$ ions was used. Such a starved reaction condition leads to the lower initial rate of polymerization.

Figure 3 shows the variation of number-average molecular weight ($M_n$) of the nitrated PTh nanoparticles with monomer percent conversion at the different $H_2O_2$ concentrations. In the case of 2.35 M $H_2O_2$, the initial rate of polymerization is fast, and the initial conversion and molecular weight are high because of the higher number of $Fe^{3+}$ ions around a micelle, as compared with the case of 5.88 M $H_2O_2$. The $M_n$ of the final products is 6011, 5882, 5792, and 5418 g/mol, respectively. All final products have comparatively lower $M_n$, which can be explained by the rigid structure of PTh molecule, confined reaction domain of micelle, and pseudo-step-growth reaction mechanism.

Table 1 summarizes the variation of particle size, degree of nitration, number-average molecular weight ($M_n$), weight-average molecular weight ($M_w$), and degree of polymerization (DP) about nitrated PTh nanoparticles by GPC and elemental analysis.[18] The degree of nitration was calculated from the nitrogen/carbon (N/C) molar ratio obtained in the elemental analysis. For example, analytical data of PTh-51 gave an N/C molar ratio of (8.70/14.01)/(30.50/12.01) = 0.98N/4C, corresponding to a degree of the nitration of 98%. Found: C, 30.50; H, 5.29; N, 8.70. Sometimes, the degree of nitration exceeded 1.00, indicating that more than one C−H group of the two C−H groups in the thiophene ring received the nitration. For example, analytical data of PTh-42 gave an N/C molar ratio of (7.24/14.01)/(23.98/12.01) = 1.04N/4C corresponding to a degree of nitration of 104%. Found: C, 23.98; H, 5.95; N, 7.24. PTh-17 gave an N/C molar ratio of (10.42/14.01)/(35.63/12.01) = 1.00N/4C, corresponding to a degree of the nitration of 100%. Found: C, 35.63; H, 6.94; N, 10.42. PTh-12 also gave a degree of the nitration >1.00 with an N/4C molar ratio of 1.04N/4C, corresponding to a degree of nitration of 104%. Found: C, 32.82; H, 11.50; N, 10.02. GPC data are shown in Table 1. As shown in Table 1, the nitrated PTh nanoparticles showed $M_n$ values of 6011−5418 (corresponding to the DP values of 47.3−40.6), $M_w$ values of 6009−5856, and the polydispersity index (PDI) values of 1.02−1.08. Consequently, we could estimate molecular weights of original PTh nanoparticles with 3879−3329 g/mol from the DP of nitrated polymers.

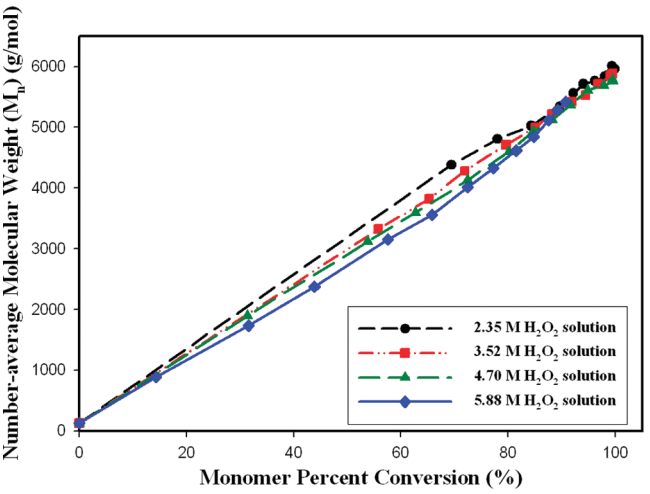


**Figure 3.** Weight average of molecular weight of PTh by the oxidant with selective hydrogen peroxide volume: 2.35 M $H_2O_2$ solution (●), 3.52 M $H_2O_2$ solution (■), 4.70 M $H_2O_2$ solution (▲), and 5.88 M $H_2O_2$ solution (♦).

**Table 1. Particle Size, Degree of Nitration, Average Molecular Weight, and Degree of Polymerization of the Nitrated PTh Nanoparticles**

| sample | particle size (nm) | degree of nitration (%)[a] | $M_n$[b] | $M_w$[b] | PDI[c] | DP[d] |
|---|---|---|---|---|---|---|
| PTh-51 | 51 | 98 | 6011 | 6249 | 1.04 | 47.3 |
| PTh-42 | 42 | 104 | 5882 | 6009 | 1.02 | 45.5 |
| PTh-17 | 17 | 100 | 5792 | 5916 | 1.02 | 45.6 |
| PTh-12 | 12 | 105 | 5418 | 5856 | 1.08 | 40.6 |

[a] $NO_2$ groups per thiophene unit; determined by N/C ratio obtained in the microanalysis (cf. the main text and the Experimental Section). [b] Determined by GPC (with polystyrene standards; eluent = THF; $M_n$ = number-average molecular weight; $M_w$ = weight-average molecular weight). [c] PDI: polydispersity index. [d] Degree of polymerization calculated from $M_n$.

FT-IR spectra of the pristine and nitrated PTh nanoparticles were measured to confirm the formation of C−N bond and N=O bond after nitration of the pristine PTh nanoparticles, as shown in Figure 4a,b. Vibrations at 1550 and 1350 $cm^{-1}$ were assigned to asymmetric and symmetric stretching in the aromatic nitro

structure (Ar-$NO_2$) of the nitrated PTh nanoparticles, as seen in Figure 4b. Intensities of nitro asymmetric and symmetric vibration bands were strong. This behavior is usually observed in aromatic nitro compounds. From these results, we can see that the nitration reaction was successfully carried out. Figure 4a,b showed the (C−H) stretching vibration band at 2931 $cm^{-1}$; (C═C) stretching band at 1450−1600 $cm^{-1}$; (C−H) in plane bending band at 1093 $cm^{-1}$; and (C−S) bending band at 741 $cm^{-1}$. These peaks are in consistency with typical peak positions of the PTh component. In addition, the doping induced band at 1066 $cm^{-1}$ originated from the changes in the conjugated backbone because of the electron-withdrawing and electron-donating dopants on the polymer chain and the counterion balancing appeared at 1093, 1350, and 1400 $cm^{-1}$.[21] The large descending baseline in the spectral region of 4000−2000 $cm^{-1}$ was attributed

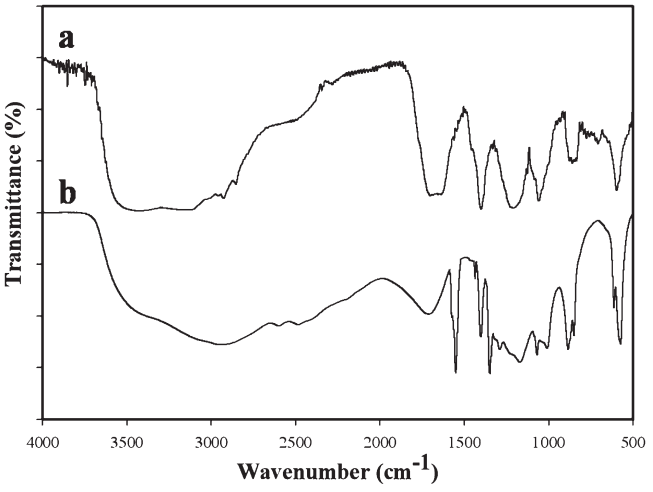


**Figure 4.** FT-IR spectra of (a) pristine PTh nanoparticles and (b) nitrated PTh nanoparticles.

because of free−electron conduction in the doped polymer. This behavior was not observed in undoped polymer.[22]

SEM and TEM (inlet) micrographs in Figure 5 show the PTh nanoparticles prepared with varying $H_2O_2$ concentration. As the $H_2O_2$ concentration increased from 2.35 to 5.33 M, the number-average sizes of the individual PTh nanoparticle significantly decreased from 51 to 12 nm. We believe that the PTh nanoparticles are nucleated within a very short time by $Fe^{3+}$ ions on the surface of the monomer-swollen micelle and they grow up with the lapse of polymerization time. Therefore, the nucleation period depends on the number of $Fe^{3+}$ ions per a micelle and again the number depends on the concentration of $H_2O_2$. As mentioned above, both rate and extent of polymerization decrease as the concentration of $H_2O_2$ increases. In fact, a drastic change in formation growth could be observed by the color change of the PTh emulsion state. In the case of the lowest concentration of $H_2O_2$ (2.35 M), a turbid and dark-red-colored latex was obtained within only a few minutes in the beginning of polymerization. A light-yellow colored latex was obtained with the highest concentration of $H_2O_2$ (5.88 M). This result showed that the overall polycondensation and coagulation rates were predominantly governed by the concentration of $H_2O_2$.

PTh nanoparticles were obtained as-prepared in a *p*-doped state at the end of the $Fe^{3+}$-catalyzed oxidative polymerization due to the oxidant (i.e., $FeCl_3$) containing $Cl^-$ dopant. Consequently, all samples were measured under the same condition, in the *p*-doped state, regardless of the effect of the doping state on the photoluminescence (PL) property. The PL intensity of the PTh nanoparticles with different particle sizes was investigated in the wavelength range of 400−600 nm, as shown in Figure 6. It was found that the PL intensity increased as the size of PTh nanoparticle decreased. This may be resulted from the variation of the total emitting area and the self-absorption effect of the PTh nanoparticles in the wavelength range of < 500 nm.[23,24] The self-absorption resulted in a transformation of the PL spectrum shape, and this result could be corroborated by the non-normalized PL spectra in Figure 6a. The total PL intensity of the PTh

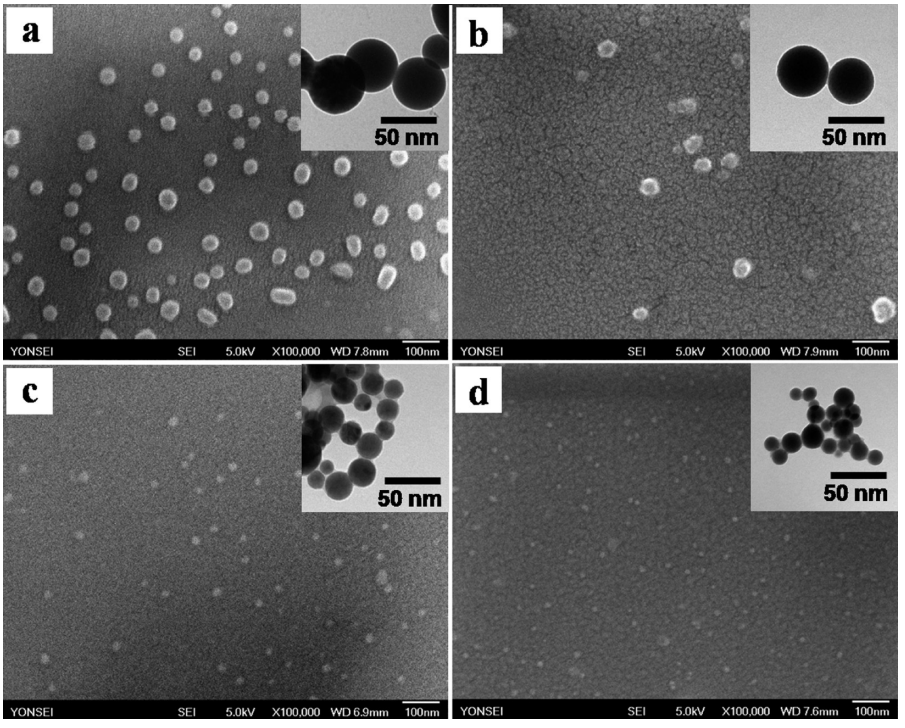


**Figure 5.** SEM and TEM (inlet) images of PTh nanoparticles prepared with various concentration of $H_2O_2$. Concentration of $H_2O_2$ and particle size of the PTh nanoparticles: (a) 2.35 M, 51 nm; (b) 3.52 M, 42 nm; (c) 4.70 M, 17 nm; and (d) 5.88 M, 12 nm.

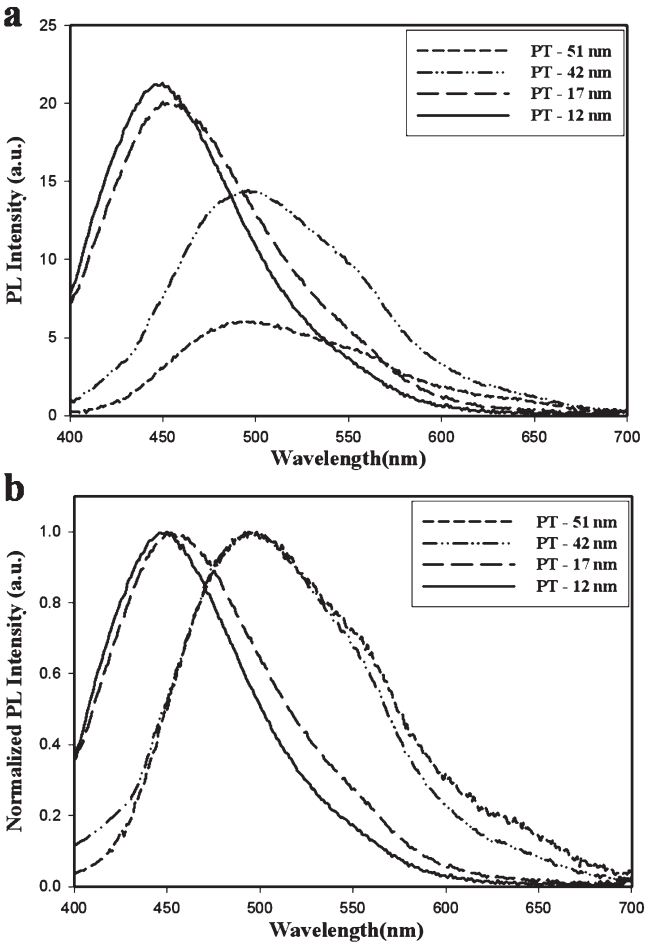


**Figure 6.** (a) Non-normalized photoluminescence (PL) spectra and (b) normalized PL spectra of PTh nanoparticle emulsions with various particle size at $\lambda^{UV}_{max}$ = 400 nm maximum absorption wavelength.

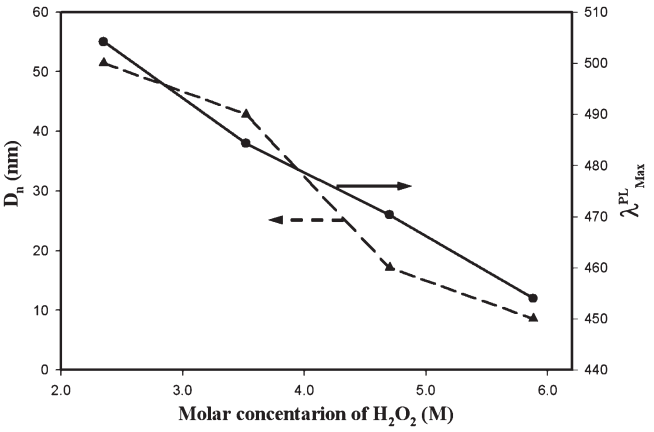


**Figure 7.** Relationship between PL maximum wavelength and particle size. As the particle diameter decreased, fluorescence spectra were slightly blue-shifted. $D_n$: number-average diameter; $\lambda^{PL}_{max}$: PL maximum wavelength.

nanoparticle increased because of the larger emitting area and lower self-absorption as the particle size decreased. In Figure 6b, the normalized PL spectrum of each sample was given to compare a shift of the $\lambda^{PL}_{max}$. The $\lambda^{PL}_{max}$ of the PTh nanoparticle showed a blue shift from 511 to 450 nm at $\lambda^{UV}_{max}$ = 400 nm absorption wavelength and the PTh concentration of $1.0 \times 10^{-3}$ M.

A relationship between the $\lambda^{PL}_{max}$ and the number-average size of PTh nanoparticle is illustrated in Figure 7. The maximum PL

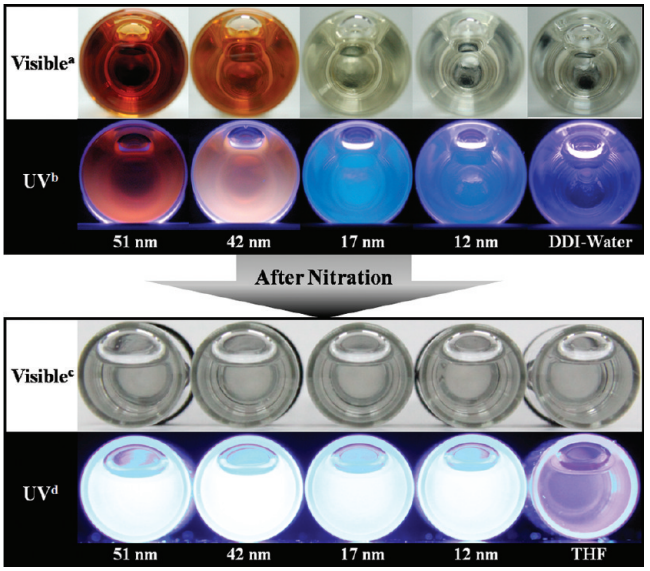


**Figure 8.** Emission color tuning of PTh emulsions and nitrated PTh solutions according to the particle diameter under visible and 365 nm UV region.

wavelength spectra ($\lambda^{PL}_{max}$) showed a blue shift as the size of the nanoparticles decreased. Until now, several mechanisms have been proposed for size-dependent spectroscopic properties in nanoparticles: (1) quantum confinement;[25−27] (2) light scattering;[28,29] and (3) lattices softening.[10,30,31] In these mechanisms, lattice softening has been suggested for organic nanocrystals, such as poly(3-[2-(*N*-dodecylcarbamoyloxy)ethyl]-thiophene-2,5-diyl) (P3DDUT),[10] perylene,[30] and pyrazoline.[31] It has been proposed that an increase in surface area results in lattice softening, which makes intermolecular interactions weaker and modifies the band gap, leading the size-dependent absorption and fluorescence properties. Therefore, it is likely suggested that lattice softening is responsible for our size-dependent spectroscopic properties in PTh nanoparticles.

Figure 8 shows the emissions of PTh nanoparticle emulsions and nitrated PTh solutions with respect to various concentrations of $H_2O_2$ under a 365 nm UV irradiation. PTh is known as a typical, red color-emitting material. However, the emission color of PTh nanoparticle emulsions was not only red but also blue under these conditions. In detail, >30 nm PTh nanoparticles exhibit red color and red emitting color under visible and UV region, respectively. PTh nanoparticles <30 nm show colorlessness and blue emitting color under visible and UV region, respectively. These results can be rationalized by the quantum confinement effect.[25−27] This color change is closely related to the size effect rather than the molecular weight of PTh. The molecular weights of all nitrated PTh nanoparticles were almost the same, and these molecules exhibit the same bright-blue color in THF solvent under the 365 nm UV irradiation. Moreover, the solutions showed the same $\lambda^{UV}_{max}$ = 316 nm and $\lambda^{PL}_{max}$ = 433 nm (Figure S3 of the Supporting Information). These data proved that the emission color of PTh depends on the particle size.

## Conclusions

We successfully controlled the size of PTh nanoparticles by manipulating the concentration of $H_2O_2$ in $Fe^{3+}$-catalyzed oxidative emulsion polymerization of thiophene. It was found that the concentration of $H_2O_2$ predominantly affected the CMC of SDS, the polymerization rate, and the corresponding size of PTh nanoparticles. The maximum PL wavelength ($\lambda^{PL}_{max}$) of the PTh nanoparticles in aqueous medium shifted in blue color from

511 to 450 nm by particle size decreasing. As the particle size decreased, the total emitting area increased, and the self-absorption of the PTh nanoparticles became negligible. Therefore, these two factors would enhance the PL intensity of the PTh nanoparticles. The results clearly prove that both absorption and fluorescence are particle-size-dependent. Most importantly, this simple method will allow the tunable emitting color of the PTh nanoparticles in various optical applications.

**Acknowledgment.** This work was financially supported by the Korean Science and Engineering Foundation(KOSEF) grant funded by the Korean government(MEST) (nos. R11-2007-050-01001-0 and 2007-0052622) and the grant from the Industrial technology development program (K0006005) of the Ministry of Knowledge Economy(MKE) of Korea. This research was supported by Nano R&D program through the National Research Foundation of Korea funded by the Ministry of Education, Science and Technology (2009-0083233). This work was also supported by the Seoul Research and Business Development Program (10816).

**Supporting Information Available:** Basic recipe of $Fe^{3+}$-catalyzed oxidative polymerization using $FeCl_3/H_2O_2$ (catalyst/oxidant) as a combination system, surface tensions of the aqueous solutions as a function of SDS concentration in $H_2O_2$ solutions, and UV-vis spectra and normalized PL spectra at $\lambda^{UV}_{max} = 316$ nm of nitrated PT nanoparticles in THF solutions with various particle size. This material is available free of charge via the Internet at http://pubs.acs.org.

## References and Notes

(1) Bao, Z.; Dodabalapur, A.; Lovinger, A. J. *Appl. Phys. Lett.* **1996**, *69*, 4108–4110.
(2) Sirringhaus, H.; Tessler, N.; Friend, R. H. *Synth. Met.* **1999**, *102*, 857–860.
(3) Andersson, M. R.; Berggren, M.; Inganaes, O.; Gustafsson, G.; Gustafsson-Carlberg, J. C.; Selse, D.; Hjertberg, T.; Wennerstroem, O. *Macromolecules* **1995**, *28*, 7525–7529.
(4) Destri, S.; Giovanella, U.; Fazio, A.; Porzio, W.; Gabriele, B.; Zotti, G. *Org. Electron.* **2002**, *3*, 149–156.
(5) Huisman, C. L.; Goossens, A.; Schoonman, J. *Synth. Met.* **2003**, *138*, 237–241.
(6) Gebeyehu, D.; Brabec, C. J.; Padinger, F.; Fromherz, T.; Hummelen, J. C.; Badt, D.; Schindler, H.; Sariciftci, N. S. *Synth. Met.* **2001**, *118*, 1–9.
(7) Theander, M.; Inganas, O.; Mammo, W.; Olinga, T.; Svensson, M.; Andersson, M. R. *J. Phys. Chem. B* **1999**, *103*, 7771–7780.
(8) Hidayat, R.; Fujii, A.; Ozaki, M.; Yoshino, K. *Jpn. J. Appl. Phys., Part 1* **2001**, *40*, 7103–7109.
(9) Xu, B.; Holdcroft, S. *Macromolecules* **1993**, *26*, 4457–4460.
(10) Kurokawa, N.; Yoshikawa, H.; Hirota, N.; Hyodo, K.; Masuhara, H. *ChemPhysChem* **2004**, *5*, 1609–1615.
(11) Kurokawa, N.; Yoshikawa, H.; Masuhara, H.; Hirota, N.; Hyodo, K. *J. Microsc. (Oxford, U.K.)* **2001**, *202*, 420–424.
(12) Kurokawa, N.; Yoshikawa, H.; Masuhara, H.; Hirota, N.; Hyodo, K. *J. Phys. Chem. B* **2002**, *106*, 10782–10785.
(13) Lee, S. J.; Lee, J. M.; Cheong, I. W.; Lee, H.; Kim, J. H. *J. Polym. Sci., Part A: Polym. Chem.* **2008**, *46*, 2097–2107.
(14) Zhao, H. B.; Li, L.; Yang, J.; Zhang, Y. M. *J. Power Sources* **2008**, *184*, (2), 375−380.
(15) Li, X. G.; Li, J.; Huang, M. R. *Chem.—Eur. J.* **2009**, *15*, 6446–6455.
(16) Belot, C.; Filiatre, C.; Guyard, L.; Foissy, A.; Knorr, M. *Electrochem. Commun.* **2005**, *7*, 1439–1444.
(17) McMurry, J. *Organic Chemistry*, 4th ed.; Thomson Brooks/Cole: Pacific Grove, CA, 1996; p 576.
(18) Yamamoto, T.; Abe, M.; Wu, B. Y.; Choi, B. K.; Harada, Y.; Takahashi, Y.; Kawata, K.; Sasaki, S.; Kubota, K. *Macromolecules* **2007**, *40*, 5504–5512.
(19) de Oliveira, B.; Bertazzoli, R. *J. Electroanal. Chem.* **2007**, *611*, 126–132.
(20) Gyenge, E. L.; Oloman, C. W. *J. Appl. Electrochem.* **2001**, *31*, 233–243.
(21) Seo, K. I.; Chung, I. J. *Polymer* **2000**, *41*, 4491–4499.
(22) Vijayan, M.; Trivedi, D. C. *Synth. Met.* **1999**, *107*, 57–64.
(23) Yamasaki, K.; Kimura, T.; Masuya, H.; Tokue, I. *Rev. Sci. Instrum.* **1997**, *68*, 3697–3701.
(24) Kim, Y. C.; Lee, T. W.; Park, O. O.; Kim, C. Y.; Cho, H. N. *Adv. Mater.* **2001**, *13*, 646–649.
(25) Alivisatos, A. P. *J. Phys. Chem.* **1996**, *100*, 13226–13239.
(26) Murray, C. B.; Kagan, C. R.; Bawendi, M. G. *Annu. Rev. Mater. Sci.* **2000**, *30*, 545–610.
(27) Glenn, W.; Heffner, D. S. P. C. L. G. *Polym. Eng. Sci.* **1995**, *35*, 860–867.
(28) Itoh, T.; Asahi, T.; Masuhara, H. *Appl. Phys. Lett.* **2001**, *79*, 1667–1669.
(29) Kreibig, U.; Vollmer, M. *Optical Properties of Metal Clusters*; Springer: Berlin: 1995; Vol. *25*, p 532.
(30) Kasai, H.; Kamatani, H.; Okada, S.; Oikawa, H.; Matsuda, H.; Nakanishi, H. *Jpn. J. Appl. Phys., Part 2* **1996**, *35*, L221–L223.
(31) Fu, H. B.; Yao, J. N. *J. Am. Chem. Soc.* **2001**, *123*, 1434–1439.